NASI.60:1274

NASA Technical Paper 1274

Erosion/Corrosion of Turbine Airfoil Materials in the High-Velocity Effluent of a Pressurized Fluidized Coal Combustor

Glenn R. Zellars, Anne P. Rowe,
and Carl E. Lowell

NASA

NASA Technical Paper 1274

Erosion/Corrosion of Turbine Airfoil Materials in the High-Velocity Effluent of a Pressurized Fluidized Coal Combustor

Glenn R. Zellars, Anne P. Rowe,
and Carl E. Lowell
Lewis Research Center
Cleveland, Ohio

EROSION/CORROSION OF TURBINE AIRFOIL MATERIALS IN THE HIGH-VELOCITY EFFLUENT OF A PRESSURIZED FLUIDIZED COAL COMBUSTOR*

by Glenn R. Zellars, Anne P. Rowe, and Carl E. Lowell

Lewis Research Center

SUMMARY

Four candidate turbine airfoil superalloys have been exposed to the effluent of a pressurized fluidized bed coal combustor operating at 0.58 meganewton per square meter (84 psia). Tests were run for up to 100 hours at two gas velocities (150 and 270 m/sec, 500 and 885 ft/sec) and at two temperatures (730° and 795° C, 1350° and 1460° F). The effluent gases had a solids loading of 2 to 4 grams per standard cubic meter (1 to 2 grains/standard ft^3). The materials tested, IN-100, U-700, IN-792, and MM-509, experienced both erosion and corrosion under these conditions.

After exposure the specimens were examined by cross-sectional loss measurement, scanning electron microscopy, light metallography, and X-ray analysis to evaluate the effects of temperature, velocity, particle loading, and alloy properties on erosion/corrosion. The results indicate that (1) erosive damage was severe and was primarily dependent on gas velocity, (2) both oxidation and sulfidation occurred at the higher temperature while oxidation of IN-100 was the only reaction at the lower temperature, (3) deposition of bed materials and erosion were observed on the same surfaces, and (4) there was little difference in the erosion/corrosion damage to the four alloys tested under these severe conditions.

INTRODUCTION

Many experts have concluded that coal, our most abundant fossil fuel, will be a major factor in meeting the nation's near-term energy needs. Our coal reserves are

---

estimated to be in sufficient supply to meet our energy needs for several hundred years. However, the potential environmental impact of expanded coal use requires that new and improved methods and technologies be developed to more fully use this energy source.

Within economic and environmental constraints, there are several near-term options for converting coal to usable energy. Indirect methods are being developed and evaluated for converting coal to gaseous and liquid fuels for use in conventional power generation systems. One advanced system that was identified in the recent Energy Conversion Alternatives Study (ECAS) (ref. 1) as having a relatively low electrical cost and being moderately efficient involves the direct burning of coal in a pressurized fluidized bed (PFB) coal combustor. In this system, granular coal is burned under pressure and at relatively low temperatures in the presence of granular limestone. The moderate combustion temperatures result in low NO_x emissions, while the chemical reactions of the combustion gases with the limestone result in low SO_2 emissions. The hot combustion gases may be expanded through a gas turbine to produce electric power in addition to the traditional production of electricity by heating steam in heat exchanger tubes to run a steam-turbine power generator. The ECAS study predicted coal-pile-to-bussbar energy efficiencies of about 40 percent; of this 40 percent the steam system accounted for about 75 percent and the gas turbine accounted for about 25 percent. Thus, the low SO_2 and NO_x emission levels combined with increased plant efficiency offer an economical means for direct combustion of the vast U.S. coal reserves that are high in sulfur.

As attractive as this method seems, it is not without serious technology problems. The gas turbine appears to be a weak link in the system, since attempts to operate a gas turbine with hot gases from direct combustion of pulverized coal have resulted in damage to turbine parts in relatively short operating times (ref. 2). Particles of unburned coal and ash were conveyed by the hot gases from the combustor into the turbine where they impacted turbine airfoils and this resulted in catastrophic erosion, corrosion, and fouling.

Laboratory and theoretical studies have provided valuable data on the erosion of candidate turbine materials and coating systems (refs. 3 to 6), on the hot corrosion of these materials (refs. 7 to 9), and in a few cases on combined effects of erosion and corrosion (refs. 10 to 11). However, since erosion processes are highly dependent on impingement angles it is difficult to predict the effect on an actual turbine from laboratory rig studies. Also, the multicomponent combination of gases and particles to be expected in the effluent of a PFB is difficult to simulate in the laboratory, as is the interaction of corrosion and erosion processes.

Since NASA has a responsibility to use aerospace technology in support of identified national needs and since the Lewis Research Center is NASA's center for gas turbine power and propulsion, an advanced design PFB has been constructed at Lewis in a

modified rocket test cell. Objectives were (1) to study the effect of the effluent gas from the coal combustor on potential gas turbine alloys and coatings and (2) to study the combustion of coal in the presence of limestone at various pressures, temperatures, and other operating parameters (ref. 12). The initial turbine materials tests reported herein were run with a simplified geometry and without gas cleanup to establish the severity of erosion/corrosion damage from this new test facility.

PRESSURIZED FLUIDIZED BED COAL COMBUSTION FACILITY

General Description

Figure 1 is an isometric drawing of the PFB test facility at Lewis. The control room is shown in the left foreground, while the high bay area on the right houses the coal and limestone hoppers, combustor, and downstream components. The coal and limestone hoppers have capacities of only 1500 and 300 kg (4000 and 800 lb), respectively, so they must be filled periodically by a charging system. The charging system uses nitrogen gas to push the coal or limestone from a tank at ground level up to the hoppers in the high bay area. The tank on the ground is filled using a forklift truck to invert and dump the 0.24-cubic-meter (55-gal) drums of 0.25-centimeter (0.1-in.) dry coal or limestone. Table I lists typical analyses of the coal and limestone used in this series of tests.

Coal Combustor

Figure 2, an artist's scale drawing of the high bay area, shows the coal combustor, the coal and limestone hoppers, the coal and limestone feed systems, and the ash cans. The combustor, seen more clearly in the schematic drawing of figure 3, consists of four principal parts: the top and bottom end caps, a cylindrical combustion or hearth section, and a conical combustion section. The cylindrical combustion section (23 cm i.d. by 91 cm high, 9 in. i.d. by 3 ft high) contains water-cooled tubes (heat exchangers) projecting horizontally into the bed to help control the operating temperatures. These heat exchanger tubes may be partly replaced with solid rod test specimens of boiler tube alloys for in-bed materials compatibility testing.

The conical combustion section varies from a 23-centimeter (9-in.) inside diameter at the bottom to a 53-centimeter (21-in.) inside diameter at the top and is 203 centimeters (6.5 ft) high. The bed designers projected that the top portion of the bed in this conical section would act like a granular filter to reduce the particulates carried out of the combustor by the combustion gases. For a given test run, the coal-limestone-ash

mixture height can be set and maintained at 61, 91, 137, 198, or 244 centimeters (2, 3, 4.5, 6.5, or 8 ft) by inserting a movable water-cooled solids removal screw in the appropriate port. This screw is shown at the fifth bed level in figure 3.

A television camera mounted in the combustor top cap permits viewing the turbulence of the bed during test operations. Water-cooled probes in the conical section permit solids to be extracted from the bed for analysis. Five sets of heat extractor tubes (called heat extractors to distinguish them from the heat exchangers in the lower hearth section) span the conical combustion chamber. These heat extractors can help to control the combustor temperatures and, like the heat exchangers, may be replaced by boiler tube alloy specimens for materials compatibility tests in the conical zone of the combustor.

A gas sampling probe is located at the top of the combustor and connected to a gas analyzer in the control room.

Carrousel Wedge Test Unit

The carrousel wedge test (CWT) unit is mounted on top of the combustor as shown in figure 3. The test unit housing is a stainless-steel 15-centimeter- (6-in.) inside-diameter tee section with three mating flanges. The bottom flange of the CWT mates with the combustor exit flange and supports a straight nozzle fabricated from Haynes alloy 25 which accelerates the combustion gases from the combustor into the erosion/corrosion test unit. The top flange of the CWT mates with the hot gas exhaust system. The third flange of the CWT mates with a flange that supports a thermocouple well for gas temperature measurement and a cold finger projection for gas condensibles. Within the test unit housing the specimen holder is fixed to an external shaft that is rotated by an electric motor through a pressure seal. The specimen holder, which accommodates eight specimens, positions the specimens directly over the nozzle 2 centimeters (0.8 in.) above the nozzle exit. In figure 4 the test specimens can be seen in the holder after a test run. The photograph is taken from the top flange; the nozzle is hidden by the specimens. The thermocouple well is seen protruding through a ceramic plug at the bottom of the photograph, but the cold finger had been removed from the unit.

Combustion Gas Exhaust System

The first stage of the combustion gas exhaust system consists of four parallel water-cooled heat exchangers that cool the gases to around 540° C (1000° F). The gases pass from the heat exchangers into a preheater and then into four cyclone separators that remove most residual particulates from the gases before venting to the atmos-

4

phere. A valve before the vent stack regulates the operating pressure within the bed.

Instrumentation and Data Acquisition

The Lewis PFB is extensively instrumented to record, monitor, and control operations. The facility was designed to operate with minimum manpower by using a programmable controller and an abort monitoring and annunciator system. Figure 5 is a schematic representation of the data acquisition, data recording, and data processing connections. The data logger receives nearly 200 responses from pressure transducers, thermocouples, and flowmeter readings located in the test cell. The data logger acquires this research data, digitizes and displays signals, logs data on printed paper tapes and a typewriter, and provides alarm set points for PFB process control. The remote collector terminal microcomputer accepts the string of characters from the data logger, puts them into an acceptable format for the central data collector, and transmits data in character synchronous mode to the data collector. The central data collector performs transmission error checking, creates a legal record of data on magnetic tape, and transmits data to the central computer in character format for research calculations.

PFB OPERATION

Atmospheric pressure feeders move coal and limestone from the respective hoppers into a blender. The coal and limestone blend is introduced into the lockhopper system and thereby fed into the high-pressure screw feeder. Air pressure pushes the coal and limestone mixture along a 0.9-centimeter (0.37-in.) tube into the bottom of the combustor, which has been filled to the desired bed height with spent limestone. The charge is fluidized by adjusting the airflow and is preheated to the coal ignition temperature by using a natural gas lance. When the coal begins to burn, the lance is turned off.

The rig is designed to burn up to 36 kilograms per hour (80 lb/hr) of coal in the presence of up to 9 kilograms per hour (20 lb/hr) of limestone to produce combustion gases low in SO_2 and NO_x. The pressure in the system can be varied from 0.14 to 0.69 meganewton per square meter (20 to 100 psia). Bed temperatures can be varied to 1100° C ($\sim 2000^o$ F), producing combustion gases around 870° C (1600° F).

During initial operation startup, while the bed temperature is rising to the desired level, the combustion gases do not pass through the CWT but are conducted into the exhaust system through an auxiliary gas vent. When the gas and bed temperatures approach the desired levels, the combustion gases are switched to the CWT path and turbine alloy materials testing begins.

TURBINE MATERIALS TEST CONDITIONS

On the basis of the initial combustion tests (ref. 12), the operating parameters were selected to test turbine alloys at two temperatures and two exhaust gas velocities. Gas temperatures were about 795° and 730° C (1460° and 1350° F). To measure average midspecimen temperatures, longitudinal holes were machined in two specimens for each run to accommodate thermocouples. The thermocouple leads were connected to a slip ring assembly on the rotating shaft. The specimen temperatures measured in this way were usually within 5° C of the gas temperature measured by the CWT thermocouple well.

Two sizes of nozzle were used to achieve the two desired gas velocities in the CWT (150 m/sec (500 ft/sec) and 270 m/sec (885 ft/sec)). For the higher gas velocity a 1.5-centimeter (0.58-in.) i.d. nozzle was used, while for the lower gas velocity tests a 1.9-centimeter (0.75-in.) i.d. nozzle was used. The airflow rate was adjusted to produce the same gas velocities at the higher temperature as at the lower temperature.

For these tests, the coal feed rate averaged 13.8 kilograms per hour (30.3 lb/hr) and the limestone feed rate averaged 2.1 kilograms per hour (4.63 lb/hr), which resulted in a calcium to sulfur ratio of 3.3. The fluidizing velocity of the gas through the bed averaged 1.3 meters per second (4.5 ft/sec) at the bottom of the combustor and 0.3 meter per second (1.0 ft/sec) at the top. Table II summarizes the effluent gas conditions within the CWT for the four materials test runs. The table was generated from test data using the continuity equation

$$V = \frac{GRT}{PA}$$

assuming one-dimensional flow through the nozzle, where V is the gas velocity, G the airflow rate, R the gas constant, T the absolute temperature, P the downstream pressure, and A the cross-sectional area of the nozzle (ref. 13).

The temperature of the effluent gas remained fairly steady through cyclic variations in the bed temperature. Gas temperatures at the top of the combustor and in the CWT are plotted in figure 6 along with total airflow for one 55-hour run. As illustrated by these plots, the beginning of each run was characterized by a period of 8 to 10 hours before final temperatures were reached; during this time heat was being absorbed by ceramic linings of the various components. Also shown in this figure is an example of an excursion (8 hr into the test) which occurred as result of an interruption in coal feed. Excursions of the opposite nature, to higher temperatures, did not occur in any of the tests reported here.

The average compositions of the effluent gases are listed in table III along with particle loadings for the four tests. Gas-borne particulates varied from 1 to 30 microm-

eters; occasionally a larger particle was found. They also varied in shape, as seen in figure 7: some had rounded shapes, while others had sharp corners and edges. An X-ray diffraction analysis identified $CaSO_4$, α-quartz SiO_2, Fe_2O_3, and various aluminum silicates. In some cases minor amounts of $CaCO_3$ or CaO were detected.

Alloys selected for testing were IN-100, U-700, IN-792, and MM-509. Master heat compositions of these alloys are listed in table IV. IN-100 was selected because it has been identified as susceptible to corrosion in laboratory tests and hence is likely to reveal if corrosion conditions exist even in the relatively short times used for these tests. IN-792 was selected because it has been identified in laboratory tests to be relatively corrosion resistant. U-700 is a blade alloy in current commercial use, and MM-509 is a cobalt-base vane alloy. In addition, these particular alloys were selected because they have been used extensively in corrosion tests at Lewis Research Center (ref. 14) and thus offer possibilities of data correlation.

Figure 8 is a drawing of the wedge-shaped specimen used for these tests. The base is held in the carrousel by a setscrew. The narrow edge on the left of the picture is designated the leading edge, while the curved surface opposite is called the trailing edge. If you look along the leading edge from the top of the picture, the side in view is called the left face and the one behind it is the right face. The carrousel wedge specimen configuration does not, of course, reproduce the range of turbine impingement angles desired. It was selected for these baseline tests because burner rig corrosion studies in this laboratory (and others) have used a similar geometry.

RESULTS AND DISCUSSION

General

Specimens exposed in the CWT to the high-velocity coal combustion products of the PFB suffered damage from both erosion and corrosion, the extent depending primarily on the velocity of the gas stream, the solids loading in the gas, the specimen temperature, and, to a lesser extent, the alloy properties.

Erosion Patterns

As a result of the geometry of the test section and the entry nozzle, the impact of the gas stream on the rotating specimens produced unevenly distributed damage. Primary material removal occurred at the center section of each specimen. Since this section was directly above the nozzle, it received the maximum impact of the gas stream and the erosive particles. As can be seen in figure 9 (photograph of test speci-

mens from the second run), the leading edges show the greatest material loss. Both faces of the wedges are eroded and the trailing edges also lost some material although they are exposed to the direct path of the stream only a third as long as the leading edges. Evidence that the direct particle paths are diverted by the specimens, which are rotating at 500 rpm, is shown by the fact that the two faces experience slightly different damage patterns. The right face suffers somewhat more damage than the left. Strong dependence of erosive damage on geometrical factors emphasizes the necessity of testing turbine materials for PFB applications in a turbine configuration.

At the end of each test the wedge specimens were removed from the carrousel, rinsed in cold water, wiped dry, weighed, measured, photographed, and then sectioned for metallographic examination. Loose dust was removed by this procedure but there remained particles of Fe_2O_3, SiO_2, and $CaSO_4$ firmly embedded in the specimen surfaces after exposure at both velocities. Figure 10 shows scanning electron micrographs (SEM) and energy dispersive spectra (EDS) of the elements present on the surfaces of two typical eroded leading edges. SEM portrays raised areas, in this case the embedded particles, as lighter than the background alloy. The EDS scans indicate calcium and sulfur from $CaSO_4$, iron from Fe_2O_3, and silicon and aluminum from aluminum silicates and SiO_2, along with titanium, chromium, cobalt, and nickel from the alloys. Oxygen does not appear on the EDS scans because it is out of range of this analysis technique.

Figure 11 is a cross-sectional view of an IN-100 specimen from the high-velocity high-temperature run in which the particles, SiO_2 in this case, have deformed the usual cubic $\gamma-\gamma'$ morphology of this alloy by the force of the impact. The gold peak identified in this and subsequent EDS scans arises from the coating applied to make the specimens conductive for SEM analyses.

Erosion Loss

The leading edge to trailing edge distance t at the center of each specimen was measured by a micrometer to a precision of ±0.001 millimeter before and after exposure. When specimen sections were mounted, this measurement was checked on a traveling microscope; the two measurement techniques agreed within ±0.02 millimeter.

Solids loading in the gas stream was determined by analyzing the samples collected for 2-hour periods in a cyclone separator and fine ceramic filter downstream of the CWT. Since initial examination of the specimens had shown that erosion was the primary mechanism of damage, the center section Δt data were divided by the average solids loading for the run to assist in comparing temperature and velocity effects.

The resulting data presented in table V and figure 12 are grouped by velocity to show the relatively small influence of the temperature differences used in these tests and the much larger influence of the gas velocity differences. Since there were generally

only two specimens of a given alloy in a particular test and no replication of test runs, no standard deviations could be calculated for these data. However, for a given test, duplicate alloy specimens agreed to within ± 0.3 (cm/yr)/(g/standard m^3). Thus, differences in alloy performance under the same test conditions are in some cases below the level of significance. The smallest loss rate in the table represents a loss of 2.1 centimeters (0.8 in.) in 10 000 hours. This loss is totally unacceptable for power turbine application. This result was, of course, not unexpected: these tests were run in order to establish a base for comparison with results after various levels of gas cleanup.

Although differences between loss rates for different temperatures and different alloys are small, the velocity effect is clear: aside from the anomalous low loss of IN-100 at the higher temperature, damage is three to seven times as great at the higher velocity as at the lower.

SEM-Metallography Studies

Scanning electron microscopy (SEM) and light metallography were employed to examine the interaction of erosion and corrosion processes.

In the first test, at 150 meters per second and 745° C for 100 hours, only IN-100 showed evidence of oxidation or corrosion as shown in figure 13. The faces and trailing edge were bordered by a depleted zone and reaction products. The leading edge, visible near the lower part of the micrograph, had evidently lost these layers by erosion. Energy dispersive spectroscopy (EDS), as illustrated by figure 14, showed that the depleted zone had lost both aluminum and chromium as compared to the alloy composition, but the reaction products contained nickel as well as aluminum and chromium and the outermost layer was nickel-rich. It is possible that the usual oxidation products of this alloy were formed initially (as indicated by the depleted zone composition) but were eroded away, leaving the later-stage oxidation products NiO and/or $NiCr_2O_4$.

In the second test, at 270 meters per second and 720° C for 45 hours, there was no evidence of oxidation or sulfidation products as seen in figure 15. If IN-100 reacted, as would be expected from the previous test results, both the reaction products and the depleted zone must have been eroded away.

In the third test, at 150 meters per second and 800° C for 91 hours, the leading edges were not sharpened as they were at the lower temperature. This was the test condition with the lightest particle loading, an anomalous Δt result for IN-100, and very uneven material removal. All the leading edges and a section of the U-700 trailing edge emerged from the carrousel with knobs of the order of 100 micrometers across and 100 micrometers high protruding from the surfaces. Figure 16 shows the U-700 trailing edge knobs in profile, head-on, and at greater magnification. Some leading

edge knobs are seen in a side view in figure 17. EDS scans of these knobs showed strong aluminum peaks such as the one in figure 17. Unfortunately, none of the knobs were captured in the cross sections prepared for metallography.

The 100-micrometer size of the knobs is much too large to correlate with hard alloy phases such as carbides. It is possible that localized erosion-resistant sites were initiated in this test run by a brief but severe excursion in total air flow (from a nominal 260 kg/hr (575 lb/hr) to over 385 kg/hr (850 lb/hr)) about 67 hours into the test.

Although the knobs may have been results of this excursion, they did not affect the erosion data because the center section loss was measured in areas between the knobs.

All four alloys developed continuous layers of reaction products and depletion zones, as seen in figure 18, on both faces and trailing edges. These layers were largely eroded away near the leading edges; a portion of the eroded area can be seen in the U-700 micrograph. The depletion zone on MM-509 is not visible in this figure because it involves a fine structure not resolved by light microscopy; it appears in SEM micrographs.

SEM examinations of the reaction product and depletion layers revealed small particles deep in the depletion zones of all four alloys: some examples of these are shown in figure 19. EDS scans suggested that these particles might be sulfides, and electron microprobe analyses confirmed that they were. An example of a probe analysis is shown in figure 20. The EDS scans suggest that in some cases the sulfides are NiS, in some Cr_2S_3, and in some both. The outer layer of reaction products appears to be a mixture of corrosion products and effluent particles.

The presence of sulfides on these alloys may have resulted from the condensation of Na_2SO_4 or K_2SO_4 on the specimens, although 800° C is near the lower threshold reported (ref. 7) for that sulfidation mechanism. Neither of those compounds was detected in the solids analyses, including a sample collected on the test section cold finger and run by atomic absorption. But, since only a trace amount of the compounds is needed to initiate the reaction, the possibility cannot be ruled out. The coal analysis does include both sodium and potassium, and the sodium did not show up downstream; however, the limestone contains aluminum silicates, which Phillips (ref. 15) suggests may be effective in tying up the alkali metals and preventing sulfate formation.

An alternative mechanism for sulfidation is reaction with gaseous SO_2. A trial calculation on the basis of equilibrium compositions (ref. 8) yielded $\log p_{S_2} = -5.3$, $\log p_{O_2} = -0.35$, and $\log p_{SO_2} = -3.0$. Although, according to the thermochemical diagrams, sulfidation should not occur with such a high oxygen pressure, it often does. The molecular gas transport mechanism in which SO_2 is carried into the oxygen-poor interior of the alloy has, for example, been reported (ref. 8) to yield sulfides with $\log p_{SO_2}$ as low as -3.1. Also, the SO_2 level on which these calculations were based is an average value which may well have been exceeded substantially for short periods.

10

In the final test, at 270 meters per second and 790° C for 36 hours, the same types of corrosion products were presumably formed as in the third test, but the reaction products were removed more rapidly at the higher velocity. Figure 21 shows one example of nickel-rich oxides underlaid by a chromium-rich region and then a depleted zone containing NiS particles. However, as seen in figure 22, most of the reaction products and depleted zones have been eroded away. Examination of cross sections near the free ends of the specimens instead of at the centers, where the temperature was perhaps lower than at the center but the erosive force was certainly less, revealed both reaction products and depleted zones as shown in figure 23.

CONCLUDING REMARKS

In summary, the initial series of materials tests in the Lewis PFB have yielded the following results:

1. As expected, erosive damage was severe. It was primarily a function of gas velocity and solids loading. Gas cleanup will be needed for power plant applications.

2. The temperature difference in these tests had little effect on erosion but did influence corrosion: both oxidation and sulfidation occurred on all four alloys at the higher temperature, while oxidation of IN-100 was the only reaction observed at the lower temperature. Thus, when the appropriate level of gas cleanup to reduce erosion to acceptable levels has been determined, hot corrosion will have to be prevented by using coatings or more resistant alloys.

3. Deposits of bed materials and erosion material loss were observed on the same specimen surfaces; they are not mutually exclusive processes.

4. Differences among the four alloys tested were slight under these severe conditions.

Lewis Research Center,
    National Aeronautics and Space Administration,
        Cleveland, Ohio, April 5, 1978,
            778-83.

REFERENCES

1. Lewis Research Center: Comparative Evaluation of Phase I Results from the Energy Conversion Alternatives Study (ECAS). NASA TM X-71855, 1976.

2. Department of Minerals and Energy, Department of Supply, Australia: The Coal-Burning Gas Turbine Project, Interdepartmental Gas Turbine Steering Committee. Australian Government Publishing Service (Canberra), 1973.

3. Finnie, Iain: Erosion of Surfaces by Solid Particles: Wear, vol. 3, 1960, pp. 87-103.

4. Clevenger, W. B.; and Tabakoff, W.: Erosion in Radial Inflow Turbines. NASA CR 134589, 1974.

5. Advanced Coal Gasification System for Electric Power Generation. Research and Development Rpt. No. 81, Westinghouse Electric Corp. Lester, Pa., 1976. (FE-1514-53.)

6. Ives, L. K.; Young, J. P.; and Ruff, A. W.: Particle Erosion Measurements on Metals at Elevated Temperatures. Prevention of Failures in Coal Conversion Systems, NBS SP-468, 1977, pp. 145-158.

7. Stringer, J.; and Erlich, S.: High Temperature Corrosion in Fluidized Bed Combustors. ASME Paper 76-WA/CD-4, Dec. 1976.

8. Birks, N.: Corrosion Mechanisms of Metals and Alloys in Multicomponent Oxidative Environments. Symposium on Properties of High Temperature Alloys with Emphasis on Environmental Effects, Z. A. Foroulis and F. S. Pettit, eds., Electrochemical Society, Inc., 1976, pp. 215-260.

9. Deadmore, Daniel L.; Lowell, Carl E.; and Santoro, Gilbert J.: High Gas Velocity Oxidation and Hot Corrosion Testing of Oxide Dispersion-Strengthened Nickel-Base Alloys. NASA TM X-71835, 1975.

10. Barkalow, R. H.; and Pettit, F. S.: Design of Materials for Use under Erosion/Corrosion Conditions at High Temperatures in Coal Gasification and Coal Combustion Systems. Rep. 75-200-7107-4, Pratt and Whitney, 1977.

11. Schaefer, A. O.: A Program to Discover Materials Suitable for Service under Hostile Conditions Obtaining in Equipment for the Gasification of Coal and Other Solid Fuels. FE-1784-21, Metal Properties Council, 1976.

12. Priem, R. J.; Rollbuhler, R. J.; and Patch, R. W.: Effluent Characterization from a Conical Pressurized Fluid Bed. Presented at 5th International Conference on Fluidized Bed Combustion, (Washington, D.C.), Dec. 1977. (NASA TM-73897.)

13. Hesse, Walter John; and Mumford, Nicholas V. S., Jr.: Jet Propulsion. Pitman, 1958.

14. Deadmore, D.; and Lowell, C.: Burner Rig Alkali Salt Corrosion of Several High Temperature Alloys. NASA TM X-73659, 1977.

15. Phillips, K. E.: Energy Conversion from Coal Utilizing CPU-400 Technology. Vol. 1 - Combustion Power, FE-1536-30, March 1977.

13

TABLE I. - COAL AND LIMESTONE ANALYSES

Constituent	Weight percent
Coal[a]	
Fixed carbon	53.92
Volatiles (including sulfur)	38.07
Sulfur	1.86
Ash:	
Silica	3.74
Alumina	2.04
Ferric oxide	1.37
Lime	.32
Phosphorus pentoxide	.03
Titania	.0⌣
Potassium oxide	.10
Sodium oxide	.03
Sulfur trioxide	.14
Magnesia	.06
Undetermined	.14
Limestone	
Sulfur	0.02
Silica	1.28
Alumina	<.10
Calcium carbonate	96.32
Magnesia	.51
Undetermined	1.77

[a]Heat content, 3.157×10^7 J/kg (13 586 Btu/lb).

TABLE II. - EFFLUENT GAS CONDITIONS IN CARROUSEL WEDGE TESTS

Run	Airflow		Temperature		Area of nozzle		Pressure		Gas velocity		Mach number
	kg/hr	lb/hr	K	°R	m^2	in^2	N/m^2	psia	m/sec	ft/sec	
I	288	635	1018	1832	2.84×10^{-4}	0.44	5.53×10^5	80.2	150	490	0.23
II	284	625	993	1787	1.68	.26	4.91	71.2	270	890	.43
III	266	585	1073	1931	2.84	.44	5.53	80.2	150	480	.22
IV	261	575	1063	1913	1.68	.26	4.91	71.2	270	880	.41

TABLE III. - SUMMARY OF TEST CONDITIONS

Run	Gas velocity, m/sec	Specimen temperature, °C	Average solids loading, g/standard m³	Average gas composition					
				O_2 (percent)	CO_2 (percent)	CO (ppm)	NO_x (ppm)	SO_2 (ppm)	THC (ppm)
I	150	745	3.9	7.7	9.5	20	122	450	2
II	270	720	4.4	7.6	10.6	14	110	420	2
III	150	800	2.3	11.7	7.5	9	231	258	2
IV	270	790	3.7	6.6	11.1	4	239	365	1

14

TABLE IV. - MASTER HEAT
ALLOY COMPOSITIONS

Element	Alloy			
	IN-100	U-700	IN-792	MM-509
	Composition, wt. %			
Ni	Balance	Balance	Balance	9.90
Co	14.90	15.50	9.20	Balance
Cr	9.30	14.20	12.70	23.4
Al	5.25	4.20	3.54	------
Ti	4.90	3.25	3.90	0.28
Ta	------	------	4.05	3.70
Mo	2.80	4.40	1.96	------
W	------	------	4.10	6.95
Zr	.08	------	.06	.46
Fe	0.21	0.10	0.18	0.32
V	.89	------	------	------
Si	.05	------	------	------
C	0.17	0.06	0.10	0.59
B	.014	.016	.015	.006
S	.002	.004	.005	.007
Hf	------	------	.80	------

TABLE V. - EROSION/CORROSION EFFECT ON CENTER
SECTION Δt DATA

Gas velocity, m/sec	Specimen temperature, ^{o}C	Solids loading, g/standard m^3	Normalized center section loss, (cm/yr)/(g/standard m^3)			
			IN-100	U-700	IN-792	MM-509
150	745	3.9	4.1	4.0	2.9	2.8
	800	2.3	.8	5.7	3.0	2.5
270	720	4.4	16.8	16.9	15.6	12.7
	790	3.7	17.7	17.1	18.7	17.2

15
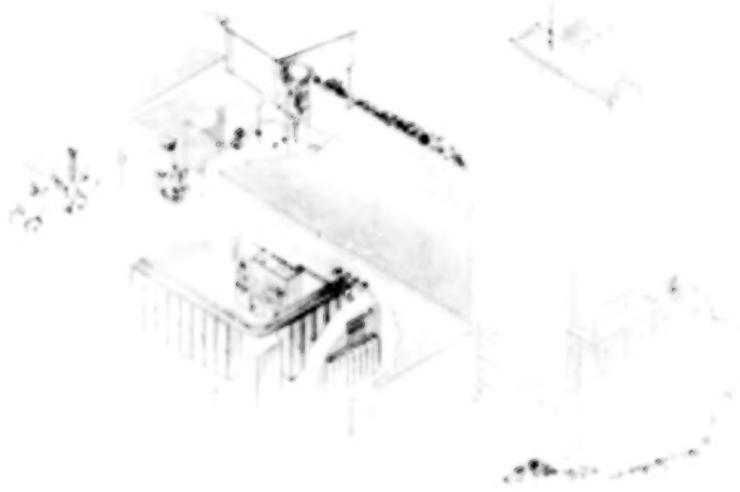
Figure 1. - Lewis pressurized fluidized bed test facility.
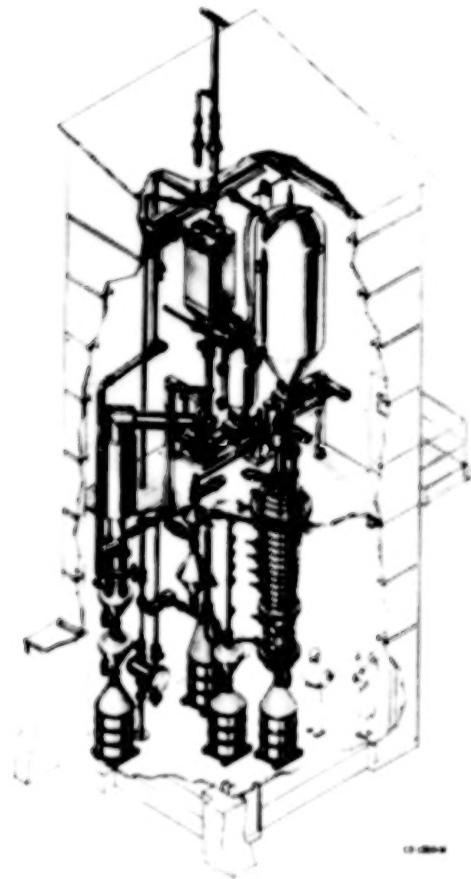
Figure 2. - High bay test area.

16
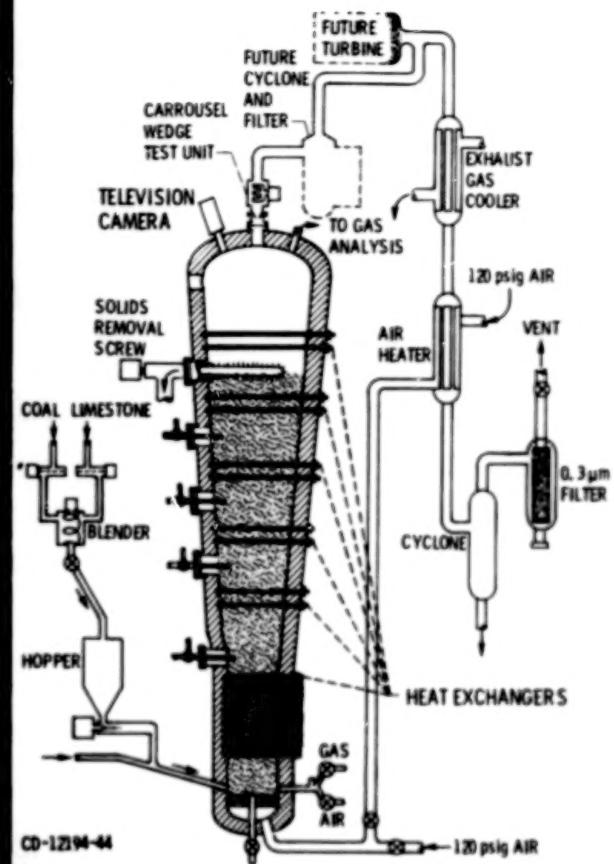
Figure 3. - Schematic drawing of combustor and auxiliary components.

Figure 4. - Carrousel wedge test unit after test.

17.
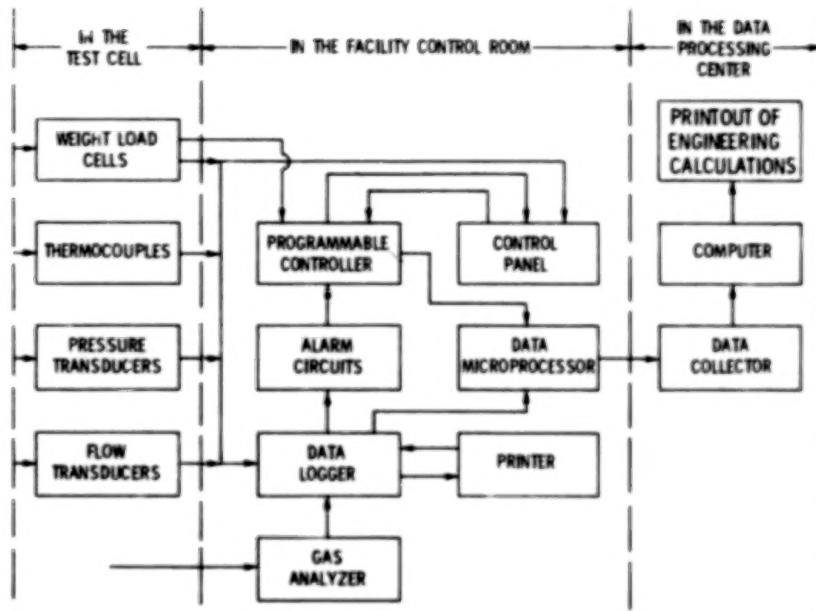
Figure 5. - Schematic of data acquisition system.
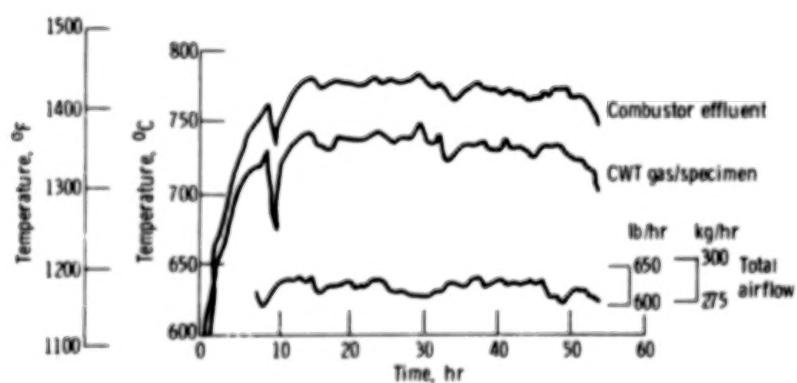
Figure 6. - Representative temperature and flow variations during the 150 meter per
second, 745° C test.
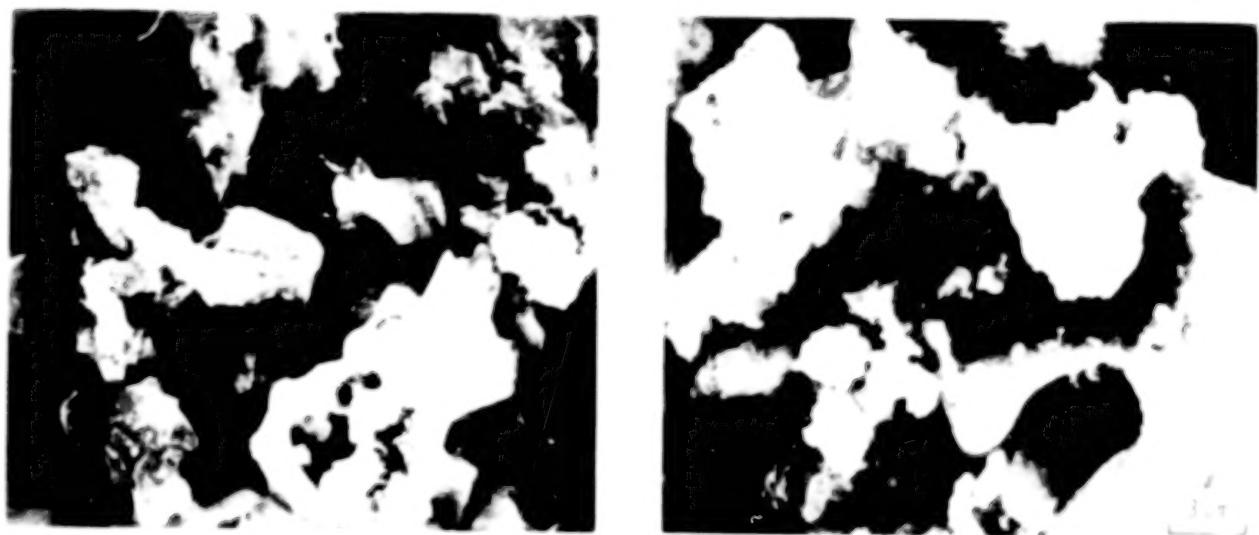
Figure 7 - Effluent particles from pressurized fluidized bed
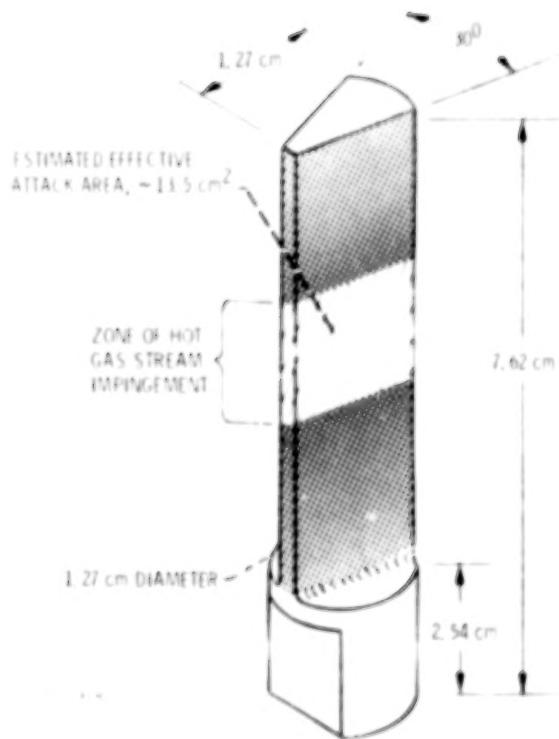
Figure 8 - Carrousel wedge test specimen

19
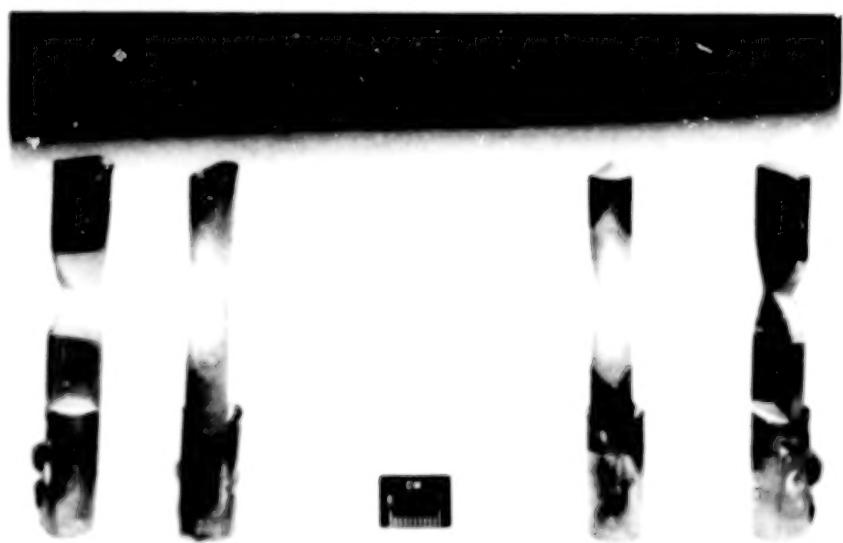
Figure 9. - Test specimens after exposure.
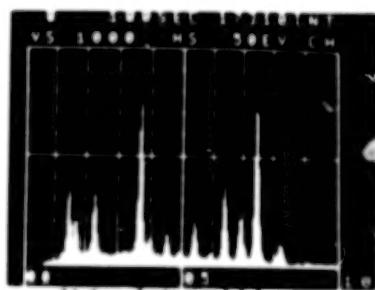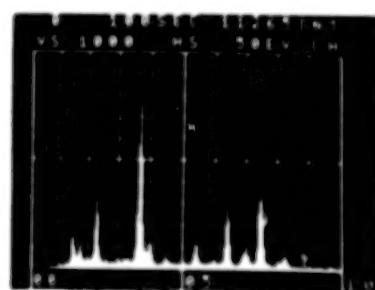
Figure 10. - Effluent particles embedded in leading edges of alloys exposed at 270 meters per second and 720° C for 45 hours.
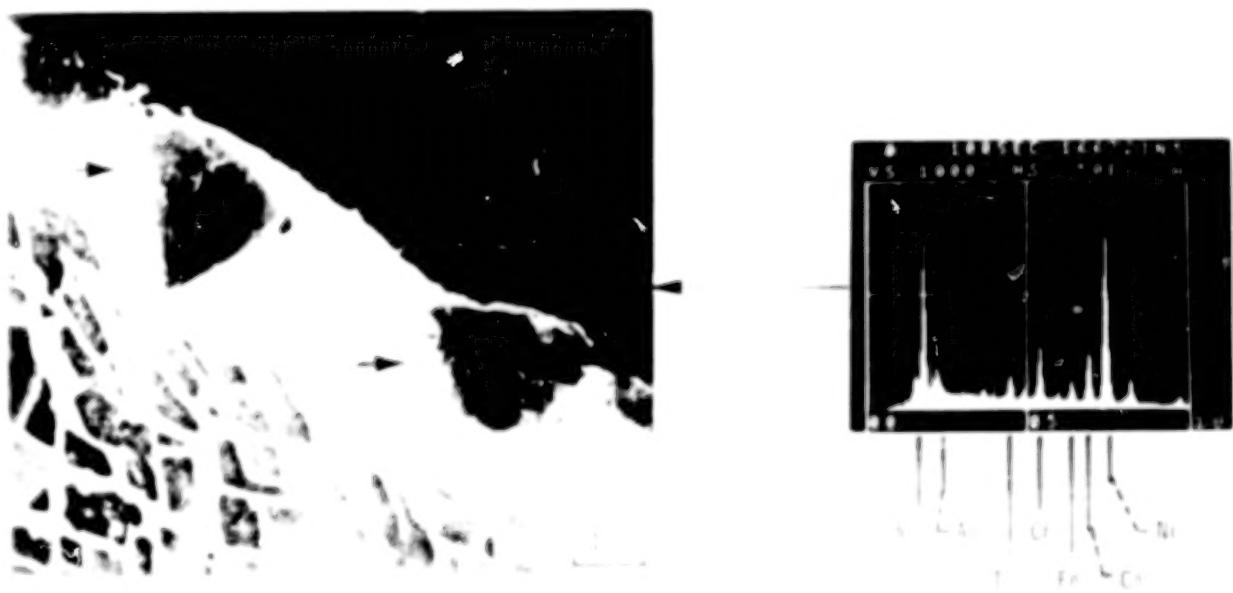
Figure 11 - Effluent particles embedded in face of IN-100 exposed at 270 meters per second and 790° C for 36 hours.
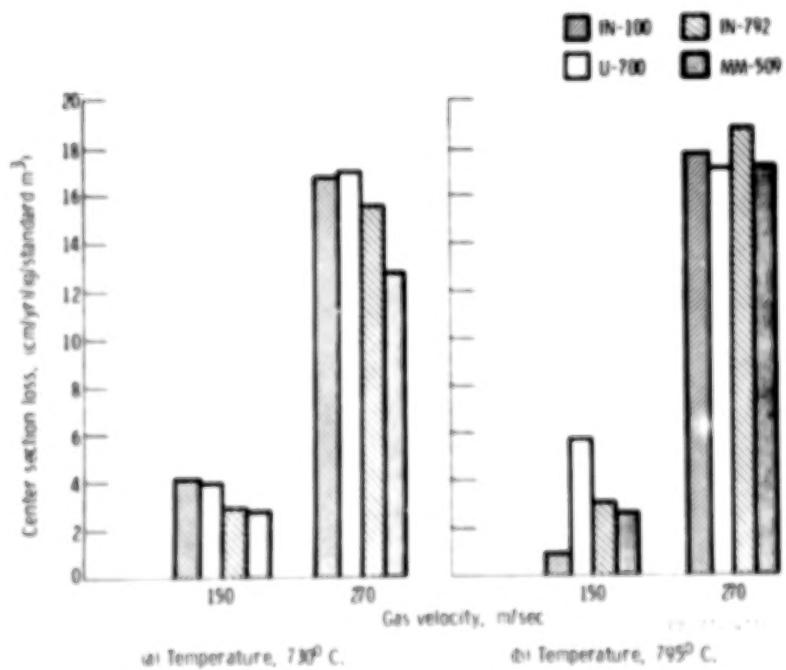
Figure 12 - Specimen center section metal loss.
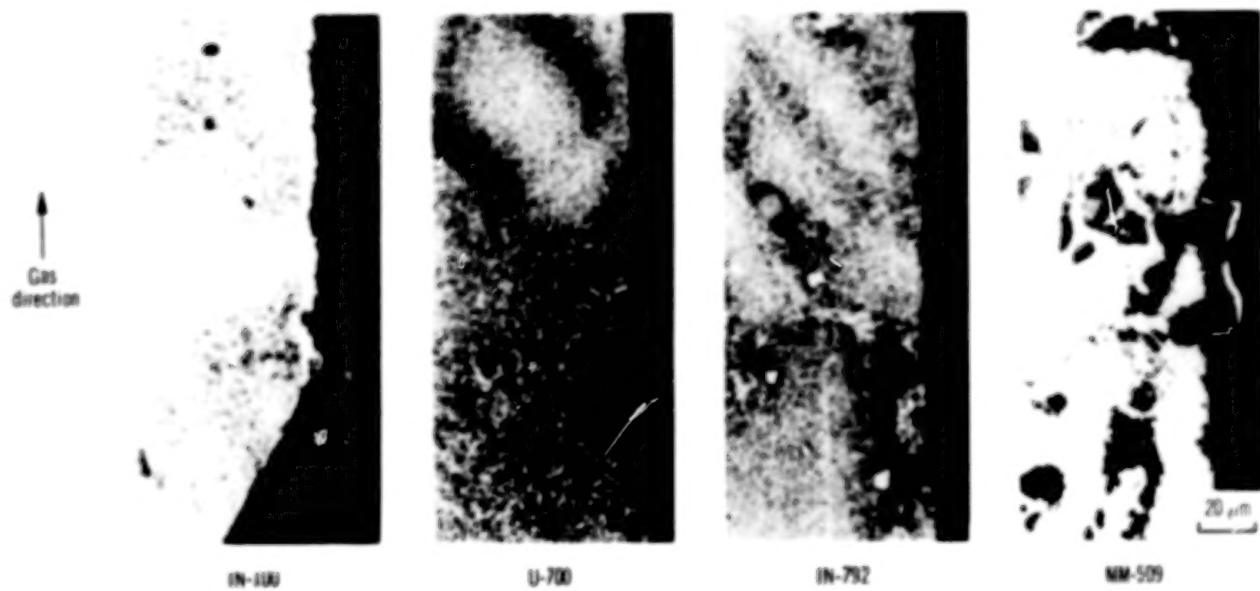
Figure 13. - Faces of alloys exposed at 150 meters per second and 745° C for 100 hours.
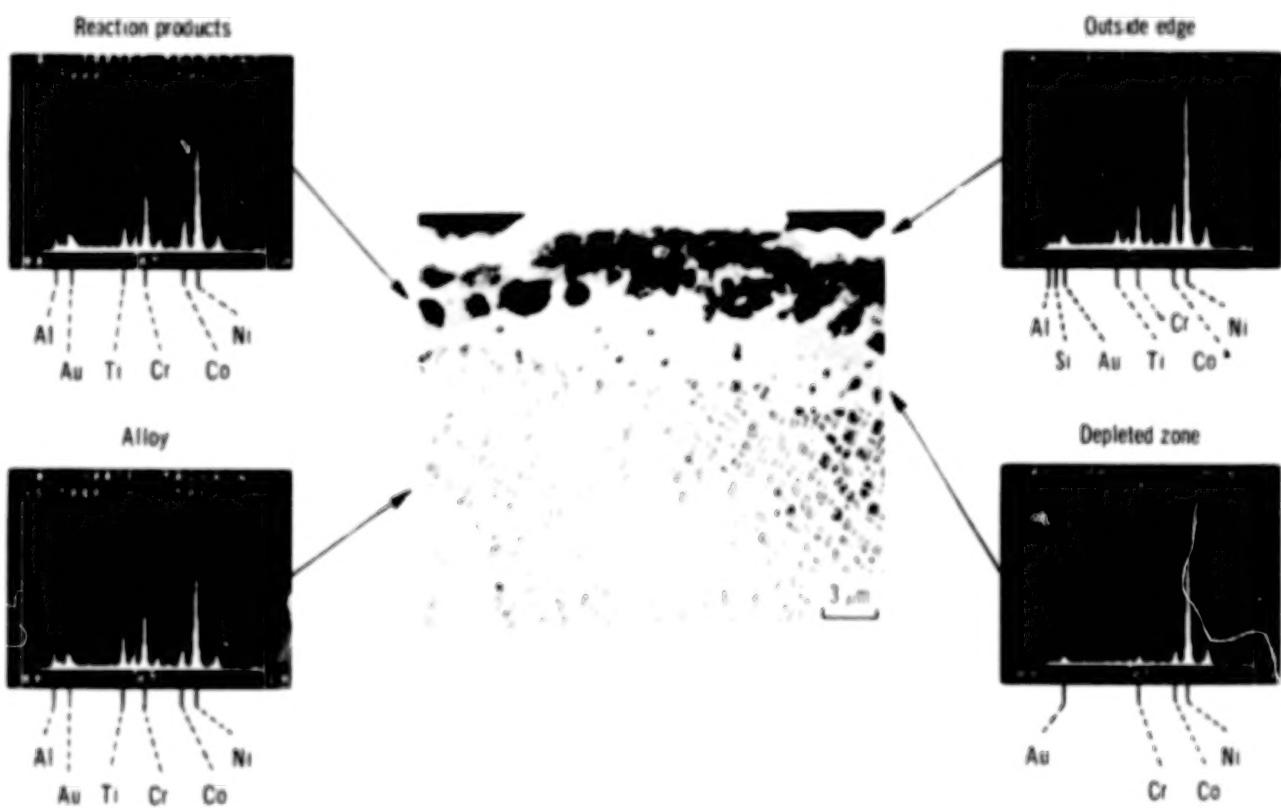
Figure 14. - IN-100 exposed at 150 meters per second and 745° C for 100 hours.

IN-100

U-700

IN-792

MM-509

← Gas direction
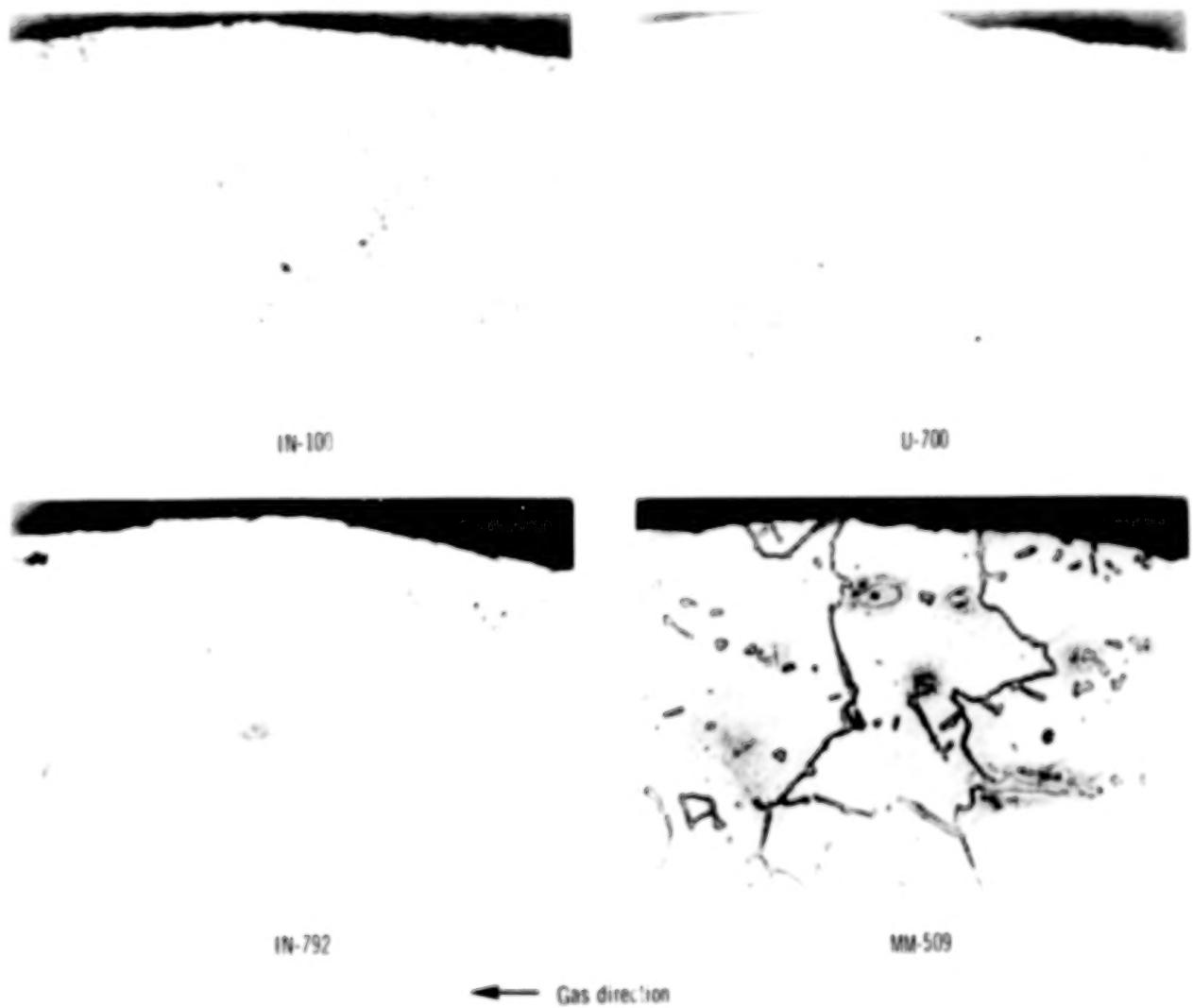
Figure 15. - Faces of alloys exposed at 270 meters per second and 720° C for 45 hours.

Left face   Trailing edge   Trailing edge
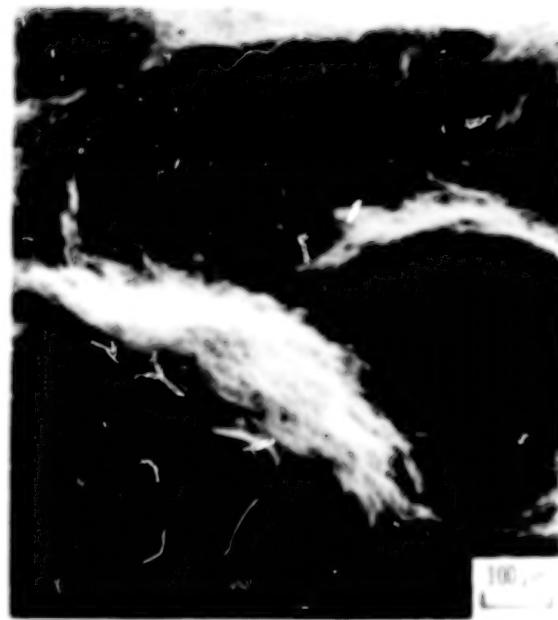
Figure 16. - Knobs on trailing edge of U-700 exposed at 150 meters per second and 800° C for 91 hours.
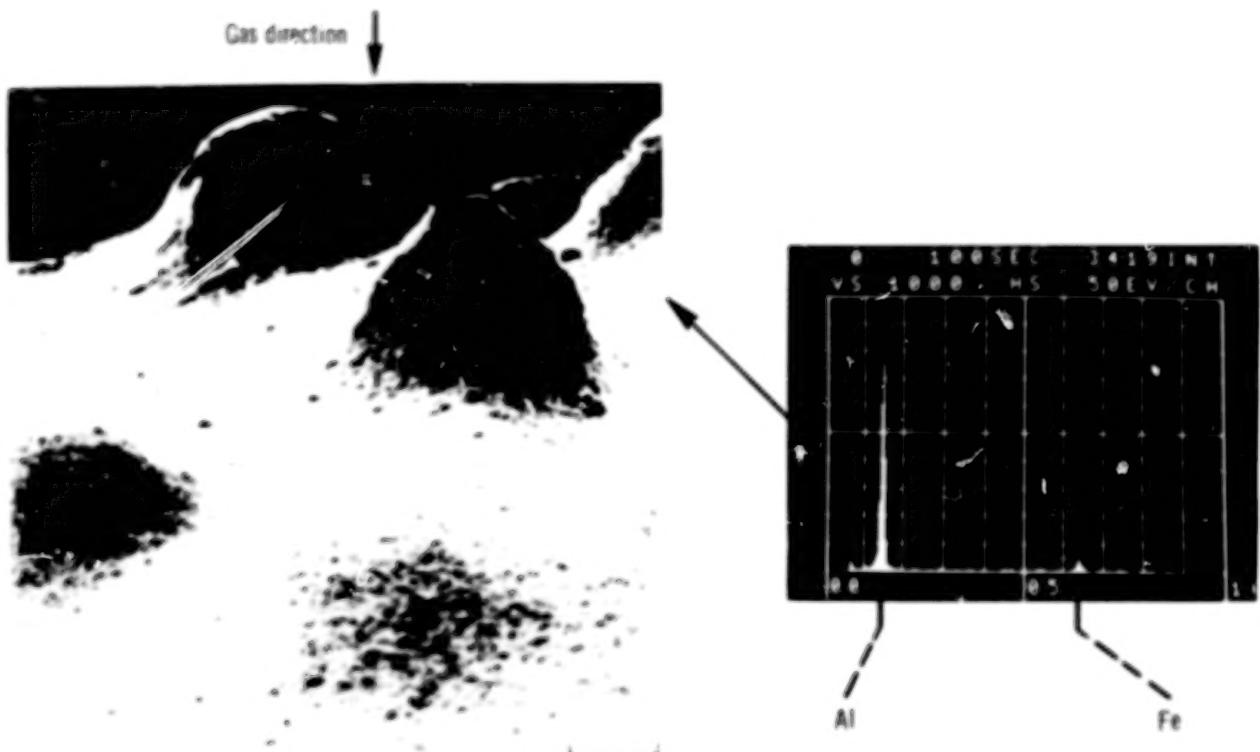
Figure 17. - Knobs on leading edge of IN-792 exposed at 150 meters per second and 800° C for 91 hours.
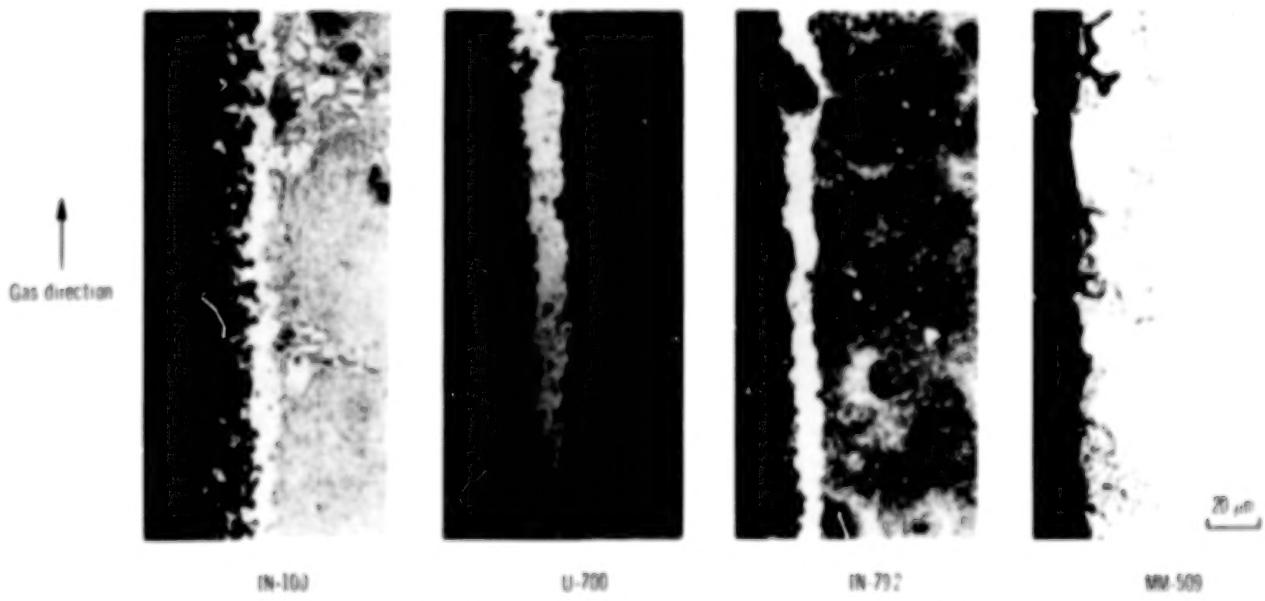
Figure 18. - Left faces of alloys exposed at 150 meters per second and 800° C for 91 hours.
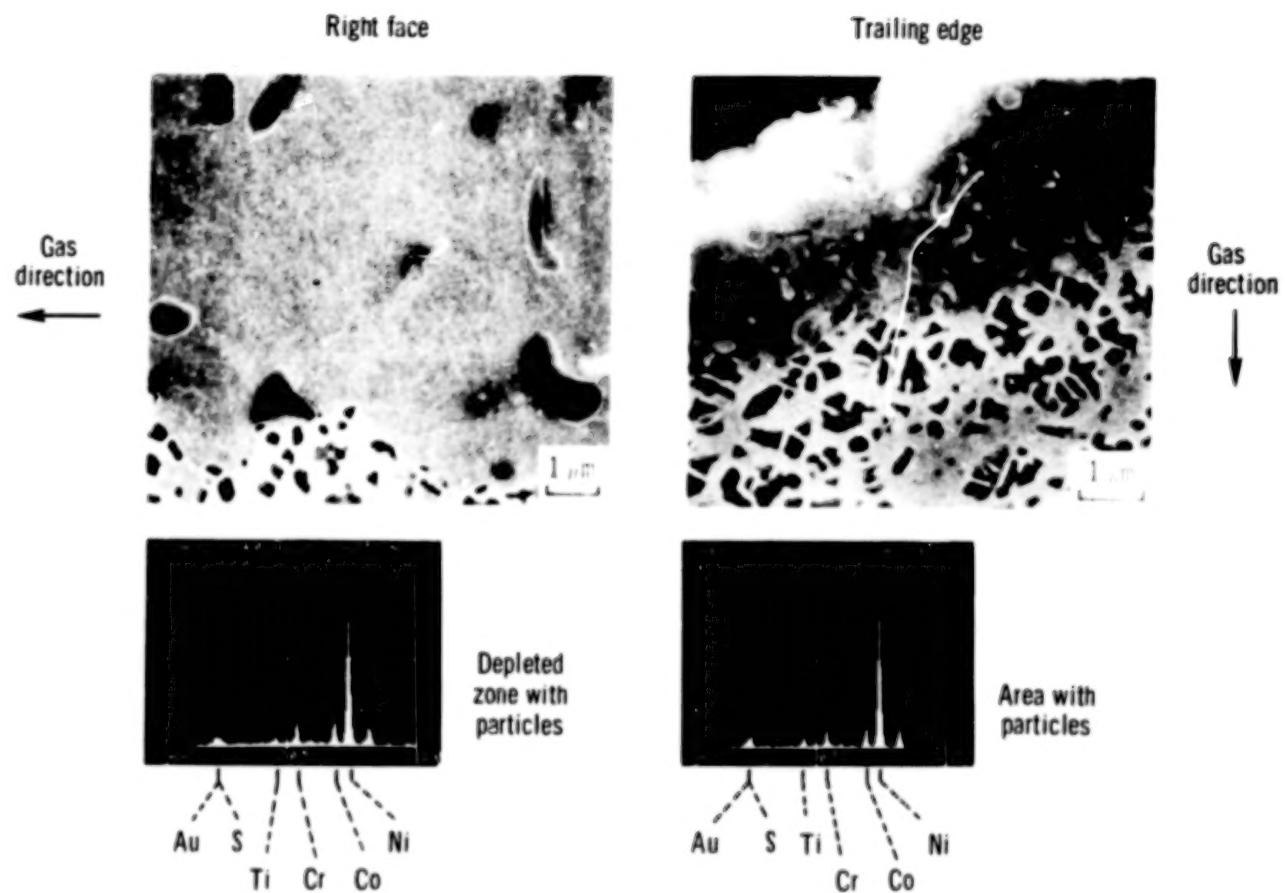
Figure 19. - Sulfide particles in depleted zone on U-700 exposed at 150 meters per second and 800° C for 91 hours.

Ni K_α X-ray scan
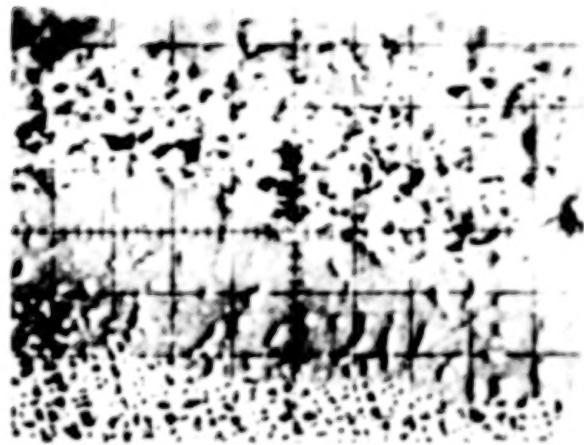
Secondary electron image
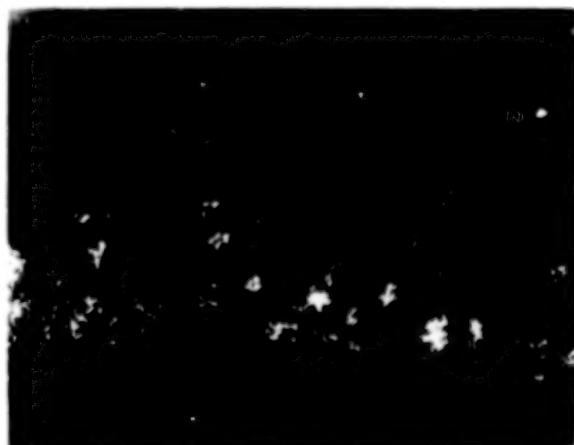
S K_α X-ray scan
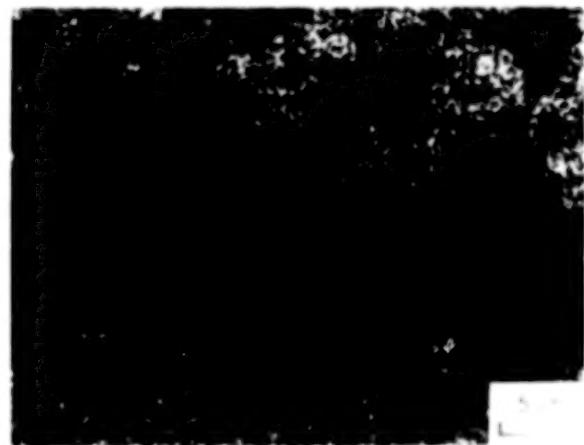
Cr K_α X-ray scan

Figure 20. - Microprobe confirmation of sulfidation on IN-100 exposed at 150 meters per second and 800° C for 91 hours.
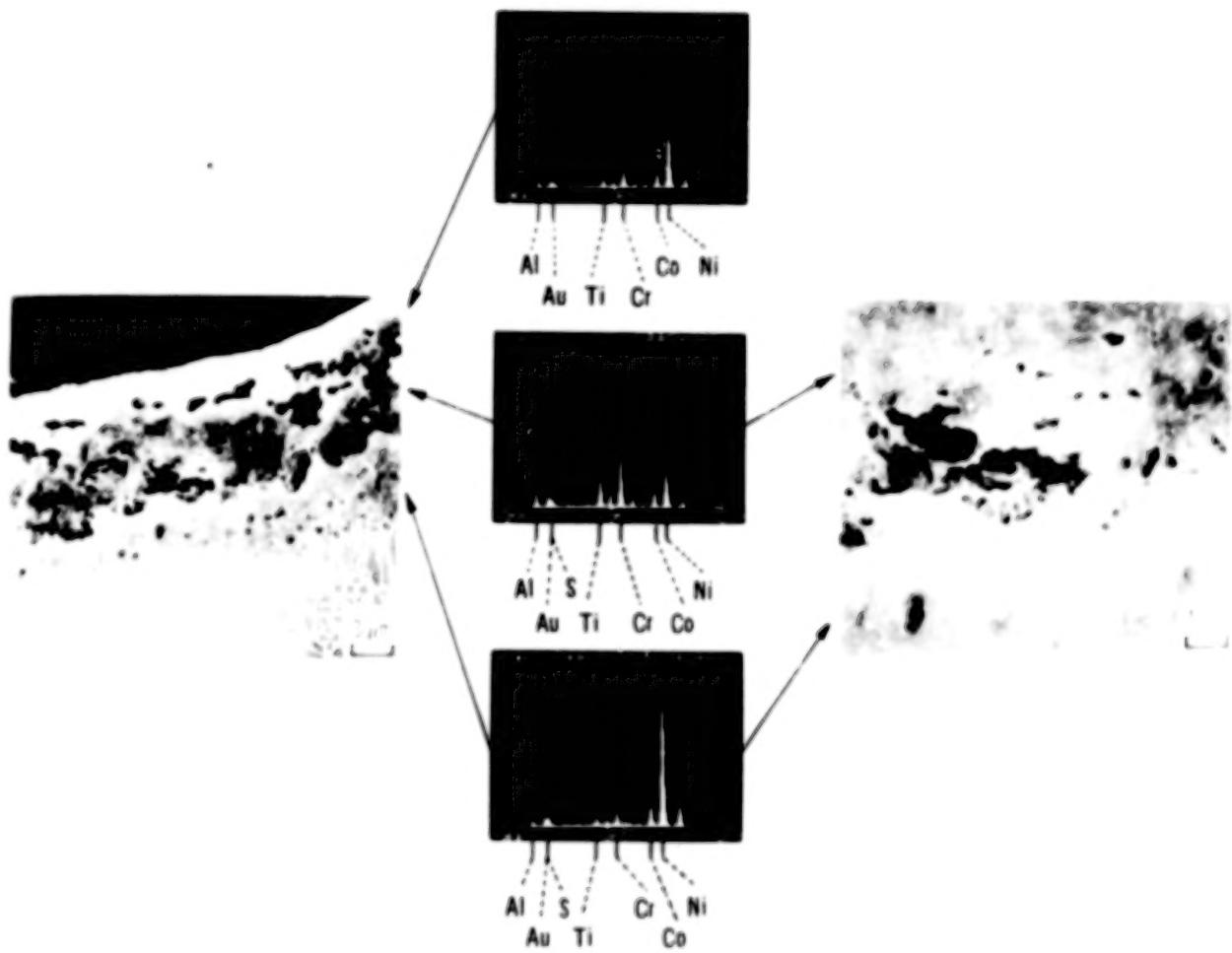
Figure 21. - Reaction products on left face of IN-100 exposed at 270 meters per second and 790° C for 36 hours.

Gas direction ↓

IN-100   U-700   IN-792   MM-509
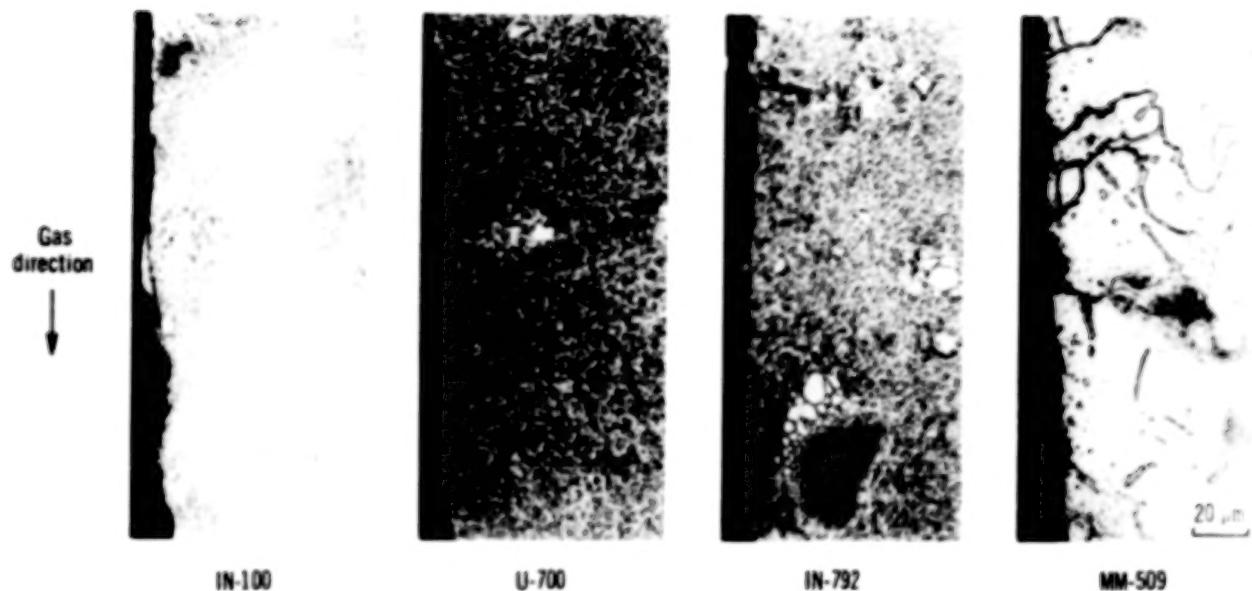
Figure 22. - Right faces of alloys exposed at 270 meters per second and 790° C for 36 hours.

Gas direction ↓

IN-100   U-700   IN-792   MM-509
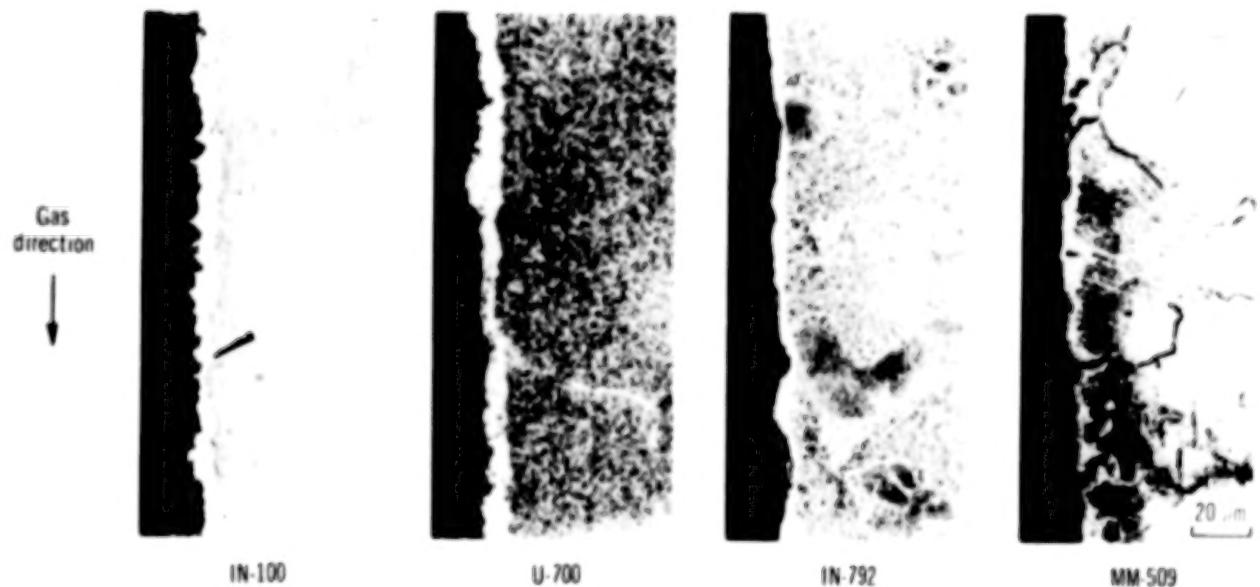
Figure 23. - Right faces near ends of alloys exposed at 270 meters per second and 790° C for 36 hours.

1. Report No. NASA TP-1274	2. Government Accession No.	3. Recipient's Catalog No.
4. Title and Subtitle **EROSION/CORROSION OF TURBINE AIRFOIL MATERIALS IN THE HIGH-VELOCITY EFFLUENT OF A PRESSURIZED FLUIDIZED COAL COMBUSTOR**		5. Report Date July 1978
		6. Performing Organization Code
7. Author(s) Glenn R. Zellars, Anne P. Rowe, and Carl E. Lowell		8. Performing Organization Report No. E-9507
		10. Work Unit No. 778-83
9. Performing Organization Name and Address National Aeronautics and Space Administration Lewis Research Center Cleveland, Ohio 44135		11. Contract or Grant No.
		13. Type of Report and Period Covered Technical Paper
12. Sponsoring Agency Name and Address National Aeronautics and Space Administration Washington, D.C. 20546		14. Sponsoring Agency Code

15. Supplementary Notes

16. Abstract

Four candidate turbine airfoil superalloys have been exposed to the effluent of a pressurized fluidized bed with a solids loading of 2 to 4 g/scm for up to 100 hours at two gas velocities, 150 and 270 m/sec, and two temperatures, 730° and 795° C. Under these conditions, both erosion and corrosion occurred. The damaged specimens were examined by cross-section measurements, scanning electron and light microscopy, and X-ray analysis to evaluate the effects of temperature, velocity, particle loading, and alloy material. Results indicate that for a given solids loading the extent of erosion is primarily dependent on gas velocity. Corrosion occurred only at the higher temperature. There was little difference in the erosion/corrosion damage to the four alloys tested under these severe conditions.

17. Key Words (Suggested by Author(s)) Gas turbine; Erosion; Corrosion; Pressurized fluidized bed; Coal combustion; Superalloys; Oxidation	18. Distribution Statement Unclassified - unlimited STAR Category 26		
19. Security Classif. (of this report) Unclassified	20. Security Classif. (of this page) Unclassified	21. No. of Pages 31	22. Price* A03

END

9. 25. 78